

Automatic on-board camera calibration on a mobile robotic system

Ramil Safin¹, Tatyana Tsoty¹, and Evgeni Magid¹

Abstract— Camera calibration is one of the important tasks in the field of robotics and computer vision. It enables to increase the accuracy of metric measurements in photogrammetry applications and provides higher performance in computer vision algorithms such as stereo matching and motion estimation. It is known that regardless of the calibration method used variation of given estimated camera parameters their is inevitable due to multiple reasons: varying weather conditions, temperature fluctuations or severe operation mode of a robotic system. In order to alleviate the aforementioned issues recalibration is required. In this work we employed 4-DoF manipulator Servosila Engineer mobile robotic system equipped with an on-board camera. In order to automate the process of calibration an algorithm is developed which enables to estimate optimal manipulator joint configurations for automatic camera calibration. Forward kinematics is solved on a discretized set of joint angles, subsequently estimating possible camera positions for its further calibration. Experiments on real robot demonstrate the possibility of usage of the developed algorithm to find optimal joint configurations for automatic camera calibration.

I. INTRODUCTION

Most of computer vision (CV) applications in robotics require a camera installed on a robotic system to be calibrated, e.g. visual simultaneous localization and mapping (SLAM) [1], structure from motion (SfM), teleoperation, path planning, obstacle avoidance [2], visual inspection [3], 3D scene reconstruction, and urban search and rescue (USAR) operations [4]. Camera calibration is the process of estimation of parameters for various camera systems, such as monocular or stereo configurations [5] [6]. Camera parameters establish a mathematical relation between 2D image and 3D world, mapping real objects in the world into pixels in an image plane. Camera calibration helps to increase the accuracy of measurements, i.e. to derive metric information from the images, hence improving performance of CV algorithms. Z. Zhang [7] distinguishes four groups of camera calibration methods : 1D, 2D, 3D, and self-calibration.

The aforementioned methods that require a particular reference object are referred to as conventional camera calibration approaches. Conversely, self-calibration approaches require neither a calibration objects nor an elaborate system setup [8]. Therefore, it is possible to use self-calibration methods in the main pipeline along with other CV algorithms, e.g. object detection and tracking. Nevertheless, self-calibration methods are prone to errors in a higher degree

¹Authors are with Laboratory of Intelligent Robotic Systems, Intelligent Robotics Department, Institute of Information Technology and Intelligent Systems, Kazan Federal University, 35 Kremlyovskaya street, Kazan, 420008, Russian Federation. The corresponding author is Ramil Safin safin.ramil@it.kfu.ru

compared to the conventional approaches [9]. 2D calibration objects, such as a checkerboard pattern or fiducial markers [10] [11], can be mounted on a mobile robot's body for further camera calibration. On the contrary, 3D calibration objects occupy more space and restrict movements of the robots, i.e. narrow down reachable workspace.

In [12] authors made use of fiducial markers for autonomous landing of UAV by continuously tracking a marker installed on a landing place. In [13] authors evaluated fiducial marker systems to compare their speed and robustness on mobile phone for AR applications. According to the criteria of fast marker detection, smooth marker tracking and detection withing 1 meter distance between the phone and markers, only two marker systems were selected: APrilTag 2 and ArUco. Markers performance was evaluated using visual assessment and shaking rate methods. Some of the design marker design attributes are considered in [14]: black to white ratio, edge sharpness, interior information complexity. Variation in marker border size affects tracking: the optimal size for borders should range from 17 to 34 percent according to the [15].

Fiala [16] proposed eleven terms for evaluating a marker tracking system: (1). The rate at which a marker is reported as present where it is,in fact, non-existent (false positive rate), (2) the rate of inter-marker confusion (ratio of wrong ID's reported to the total number of ID's reported), (3) the rate at which the system misses the detection of a marker which present in front of camera (the false negative rate),(4) the marker minimal size(the possible minimal size of the marker which is reasonable for detection), (5) the characteristics of vertex jitter (i.e. noise ratio in marker), (6) the library space (the total number of fiducial stored as templates in the library), (7) handling the change in lighting conditions, (8) handling occlusion, (9) the performance speed, (10) perspective support, and (11) handling photometric calibration.

In [17] advantages of combining fiducial markers into a board are highlighted - marker detection in case of partial occlusions and varying distances. There are works where different fiducial markers are compared. For example, in [18] authors compared ARTag, AprilTag, ArUco, and STag using motion capture system as a reference for the ground truth. Markers were evaluated at varying distances and illumination conditions. The best detection rate is shown by AprilTag. In terms of precision when it comes to position measurements STag presented the best results in all cases, AprilTag shows the best results in orientation measurements.

In one of our previous works we compared ArUco and AprilTag systems for rotation resistance under noise presence

[19]. Where ArUco markers showed superiority in case of rotations in presence of Gaussian noise. In [20] authors presented an automatic multi-camera calibration method. The setup consists of 4 fixed cameras in the lab room above the robot workplace. They used a robot to automate the intrinsic camera calibration attaching a marker on its manipulator. For extrinsic camera calibration two small markers were used which were attached to the robot base.

There are fiducial markers, which help to improve accuracy and mitigate issues related to partial occlusions and illumination condition. There are works on improved chessboard patterns, some of them suggest to use electronic devices as a source of calibration patterns [21]. Electronic patterns potentially benefit from the ability to dynamically change markers size and image resolution. There are other advanced camera calibration techniques which try to enhance the accuracy of the camera parameters estimation in different environments. For example, spherical calibration objects can be used to lessen calibration pattern occlusion issues [22], whereas checkerboard pattern can be further modified to increase the accuracy of calibration in different light conditions using additional structural elements [23].

In this work a mobile robot with 4-DoF manipulator is employed. It is equipped with four cameras installed on the robotic head. In order to be utilized in USAR related tasks, particularly, in visual inspection and 3D scene reconstruction of the destructed buildings or debris, cameras are required to be calibrated. Given estimated camera parameters – regardless of the chosen calibration approach – continuous changes in camera parameters during operation are inevitable. There might be multiple reasons for that, such as a varying weather conditions (for instance, changes in temperature and air pressure) and severe operation mode. Consequently, these factors lead to the accuracy and performance degradation. Thus, in order to mitigate a variation in visual sensor parameters a recalibration step is required.

In order to alleviate the camera parameters degradation issues we propose our solution which encompasses automatic camera calibration with on-board markers mounted on the mobile robot's body. One of the steps of 2D object-based calibration is a relative motions between a camera and a marker. For instance, in checkerboard calibration method the pattern should be viewed in at least 3 different positions relative to the camera. Therefore, it is necessary to estimate robotic arm joint configurations, i.e. find angles between the links of the manipulator, where camera can detect marker from various distances and angles. In our algorithm we solve for forward kinematics on a discretized set of joint angles. Subsequently, some of the estimated camera positions are manually checked so the camera can detect the marker. Conducted simulations and real pilot experiments demonstrated the algorithm's usability for further camera calibration.

II. ROBOT MANIPULATOR KINEMATICS

In our work we employed Servosila Engineer crawler-type mobile robot (Fig. 1) which is primarily designed for USAR

operations [24]. It is equipped with four cameras located on the built-in 4-DoF manipulator.

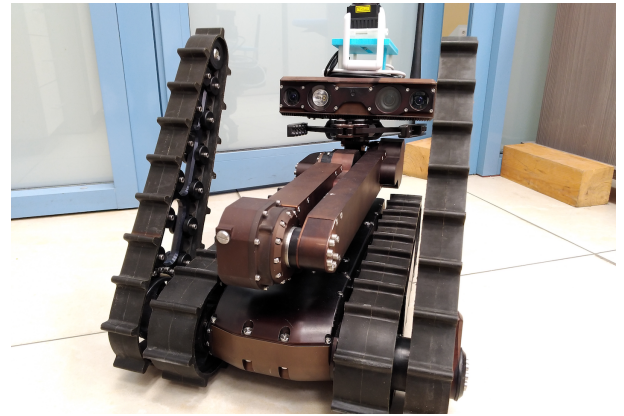


Fig. 1. Servosila Engineer crawler-type mobile robot (front view).

TABLE I
D-H PARAMETERS DESCRIBING KINEMATICS OF THE SERVOSILA
ENGINEER'S MANIPULATOR (EACH ROW DESCRIBES A
TRANSFORMATION FROM $(i-1)^{th}$ TO i^{th} LINK).

i	r_i (mm)	α_i (rad)	d_i (mm)	θ_i (rad)
1	70	$\pi/2$	0	θ_1
2	300	0	0	θ_2
3	425	0	-60	$\theta_3 + \pi$
4	0	0	60	$\theta_4 - \pi$

Forward kinematics (FK) touches upon the problem of determining end-effector's position and orientation for the given joint variables (angles). Denavit-Hartenberg's (DH) notation can be used to describe a kinematic chain, i.e. four parameters describing the relationship between adjacent links of a manipulator:

- r_i – link length, the distance from the Z_{i-1} to the Z_i axis along the X_i axis;
- α_i – twist, the angle between Z_{i-1} and Z_i axes around the X_i axis;
- d_i – offset, displacement from the X_{i-1} to the X_i axis along the Z_{i-1} axis;
- θ_i – the angle between X_{i-1} and X_i axes around the Z_{i-1} axis.

Model of Servosila Engineer's kinematic chain is demonstrated in Fig. 2. Each link is assigned with a coordinate frame, where Z_{i-1} is the axis of rotation of the i^{th} link. The transformation from the $(i-1)^{th}$ to the i^{th} link is described by the i^{th} row in Table I. It represents the following 4x4 homogeneous transformation matrix ($c \equiv \cos$ and $s \equiv \sin$):

$${}_{i-1}^i T = \left(\begin{array}{ccc|c} c\theta_i & -c\alpha_i \cdot s\theta_i & s\alpha_i \cdot s\theta_i & c\theta_i \cdot r_i \\ s\theta_i & c\alpha_i \cdot c\theta_i & -s\alpha_i \cdot c\theta_i & s\theta_i \cdot r_i \\ 0 & s\alpha_i & c\alpha_i & d_i \\ \hline 0 & 0 & 0 & 1 \end{array} \right) \quad (1)$$

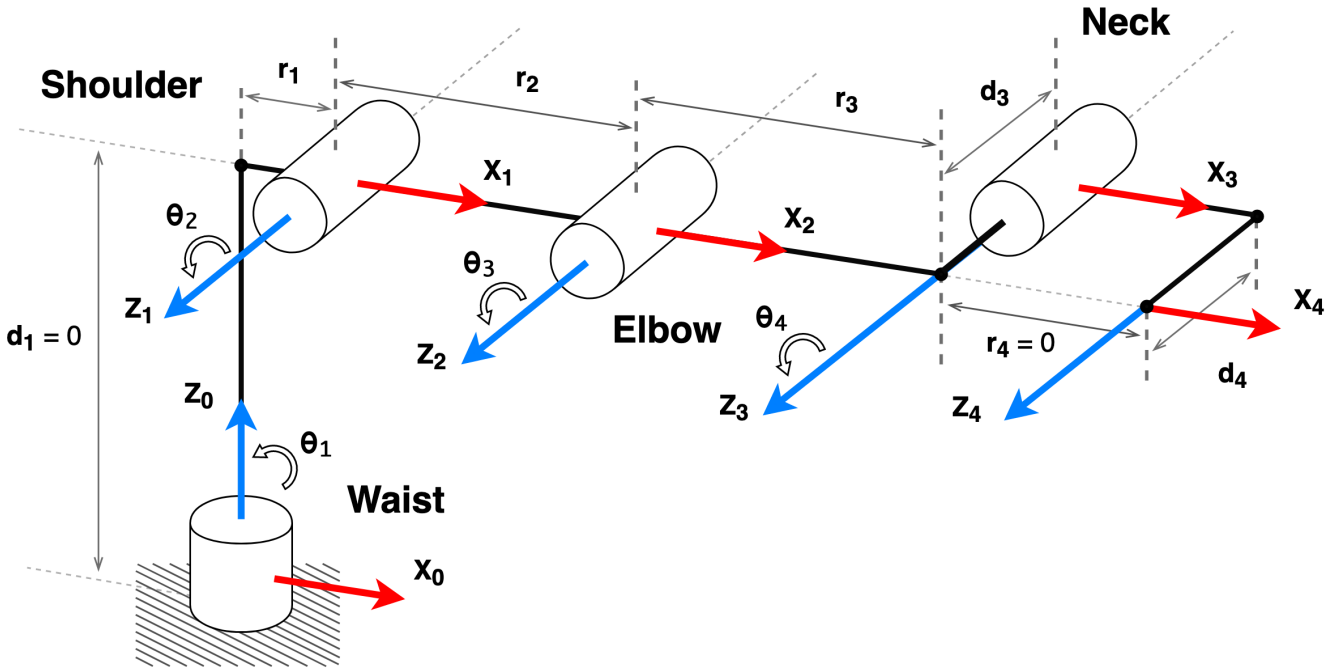


Fig. 2. Sketch of the Servosila Engineer's 4-DoF manipulator. Each link (black line) is attached with a (right-handed) coordinate system with the origin in the center of the revolute joint (cylinder). Z_i is the axis of rotation and θ_i is a positive direction of rotation for the i^{th} joint. Link length and offset are denoted as r_i and d_i , respectively. ($X_4 - Z_4$) coordinate frame represents the end-effector of the manipulator (e.g. camera).

or

$${}_{i-1}^iT = \begin{pmatrix} {}_{i-1}R^3 & {}_{i-1}t \\ 0^3 & 1 \end{pmatrix},$$

where ${}_{i-1}t$ – a translation vector from the $(i-1)^{th}$ to the i^{th} frame origin and ${}_{i-1}R^3$ – a 3x3 rotation matrix (orientation). Thus, given joint angles (θ_i , $1 \leq i \leq 4$), end-effector's position and orientation, i.e. forward kinematics, can be computed as the product of homogeneous transformations (from the 0^{th} to the 4^{th} frame):

$${}_0^4T = {}_0^1T \cdot {}_1^2T \cdot {}_2^3T \cdot {}_3^4T \quad (2)$$

Obtained DH parameters are used to build a model of the robotic arm in MATLAB. Particularly, we make use of Robotics Toolbox for visualization purposes and to solve for forward kinematics [25] (Fig. 3). Moreover, we employ DH parameters in order to solve for boundary singularities.

III. AUTOMATIC CAMERA CALIBRATION ALGORITHM

Developed automatic on-board camera calibration algorithm considers the following factors:

- static stability of the mobile robotic platform – can be disrupted during operation especially if the projection of the robotic head is outside of the support polygon (SP). In order to mitigate this issue we propose to extend the SP by turning flippers to the front (Fig. 6);
- singularity configurations on the workspace boundaries – singular configurations must not be considered for further calibration process;

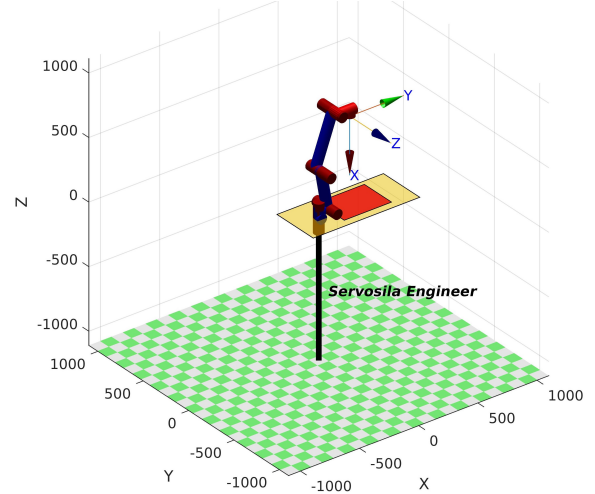


Fig. 3. Camera looking at the calibration pattern (in red).

- detection possibility of the calibration pattern – on-board camera's viewing vector must be directed towards the attached to the robotic platform calibration pattern.

After analysis of possible marker positions on the mobile robot, considering possible marker size and ability of detecting it from different positions and orientations, it was decided to fix it on the robotic base above the battery section [26]. We estimate positions and orientations of the robot manipulator's end-effector in which a marker with a high probability can be detected by the camera:

- Specify the position and dimension of the marker on the robotic base (Fig. 3, red zone).

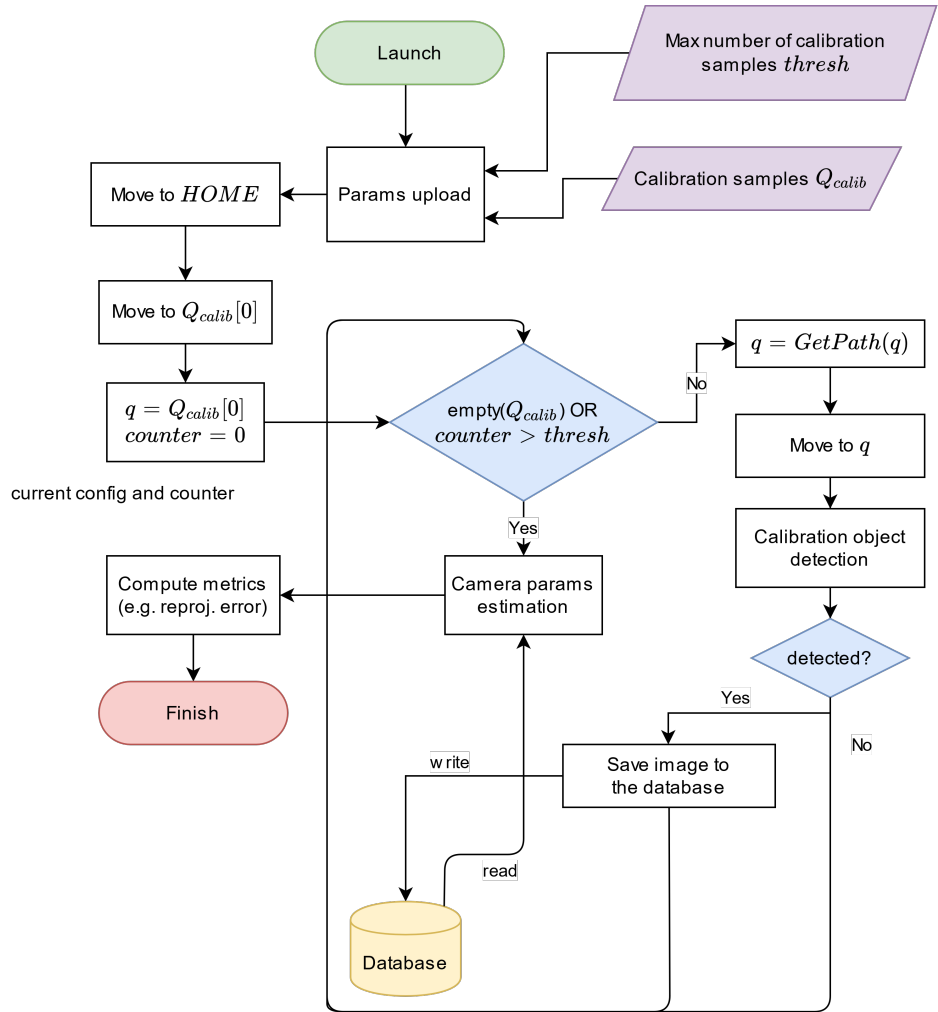


Fig. 4. Automatic camera calibration flow chart.

- Exhaustive search – given reference joint angle limitations, go through the range of discretized joint angles (starting from the minimum angle up to the maximum one) and compute the position and orientation of the end-effector (camera), i.e. solve for FK for each joint configuration.
- Given camera view direction, which is considered to be end-effector's X -axis (Fig. 3), determine its coordinates with respect to the manipulator's base frame.
- Compute the intersection point of the end-effector's X -axis and marker plane. We distinguish three cases depending on the location of the projection point: outside the marker zone, on the edge (vicinity) of the marker zone, and inside the marker zone. Points which are outside the zone are filtered out immediately, whereas points which are close the edges are kept for further analysis.
- Clustering. Total number of possible solutions is reduced up to around 200 configurations by applying K-means clustering algorithm (Fig. 5).

As a result we have a set of configurations which can

be potentially used in the automatic calibration routine. The developed automatic calibration algorithm moves the manipulator along estimated configurations at the same time collecting image data for camera calibration.

IV. EXPERIMENTS

A. Methodology

The algorithm method for the intrinsic camera calibration partially follows the method proposed by Zhang. This calibration algorithm makes use of multiple images of an chessboard-based pattern taken from different viewing angles and distances. Given N images of the planar calibration object the equations are joined to get a homogeneous system of linear equations which can be solved when $N \geq 3$.

The calibration pattern consists of chessboard cells arranged in a grid and Chilitag markers built inside black cells (Fig. 7). We chose Chilitag according to our previous research work [26]. The dimensions of the pattern are 10×10 cm.

To collect all images needed for the calibration process, we use a list of predefined poses (a total of 50 different poses

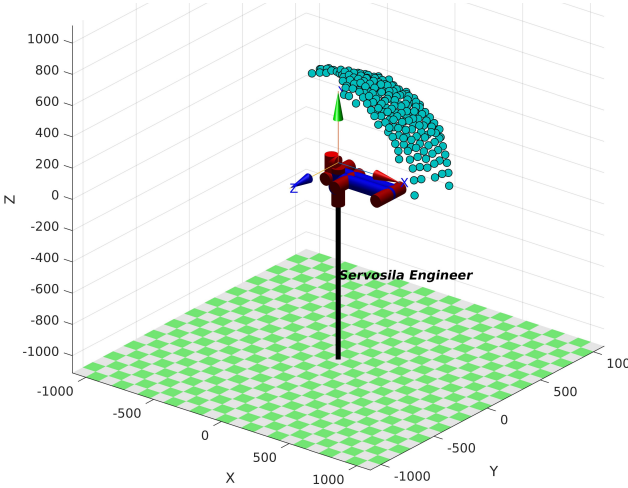


Fig. 5. A set of possible manipulator configurations after clustering.

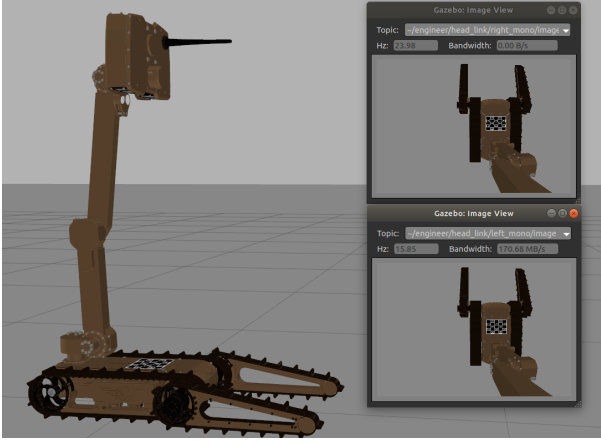


Fig. 6. Servosila Engineer mobile robot in simulation environment. Calibration pattern is attached to the mobile platform.

with high geometric variation over the entire workspace) for the robot. Variability of poses is guaranteed by the clustering step of all possible on-board camera poses. Those poses were arbitrarily selected from the set of safe poses.

We conducted 20 experiments with the same initial conditions in simulation environment with even illumination and no shadows. The simulation environment was built in Gazebo. Robotic arm moved along predefined waypoints (configurations) using MoveIt! Framework capabilities (path planning and execution). In our experiments we measured the following quantities: execution time, memory consumption, number of calibration samples.

B. Results and Discussion

The average execution time of the automatic calibration algorithm is around 315 seconds. The additional delay is introduced at each waypoint in order for a camera to be able to capture the image while being stationary. This mitigates possible issues with marker detection due to motion blur.

Memory consumption grows linearly with the growing number of calibration samples stored. Overall, no memory

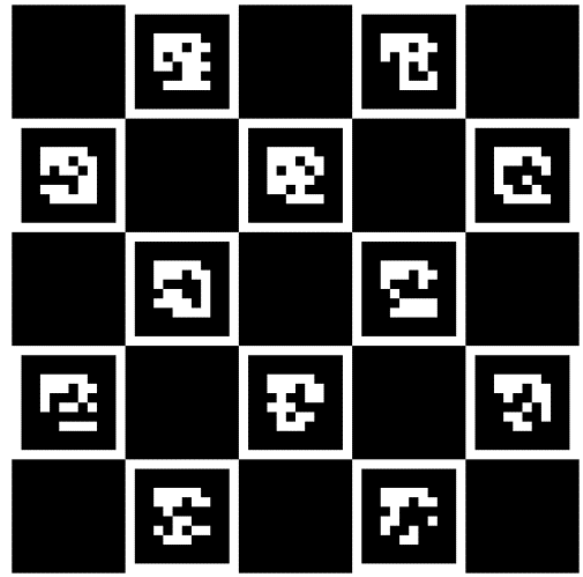


Fig. 7. Chilitag markers arranged in a chessboard grid forming a camera calibration pattern.

leaks were detected, and the resulting average memory consumption was around 200 MB. Average number of valid calibration samples was around 70%.

As for the calibration quality, the resulting average re-projection error estimated to 0.532 pixels. This is a fair result for a calibration algorithm. The accuracy of the algorithm depends on the number of calibration samples provided, the distance to the calibration pattern, and the image resolution.

ACKNOWLEDGMENT

The reported study was funded by RFBR, project number 20-38-90257.

REFERENCES

- [1] E. Mingachev, R. Lavrenov, T. Tsot, F. Matsuno, M. Svinin, J. Suthakorn, and E. Magid, "Comparison of ros-based monocular visual slam methods: Dso, ldso, orb-slam2 and dynaslam," in *International Conference on Interactive Collaborative Robotics*. Springer, 2020, pp. 222–233.
- [2] C. Brand, M. J. Schuster, H. Hirschmüller, and M. Suppa, "Stereo-vision based obstacle mapping for indoor/outdoor slam," in *2014 IEEE/RSJ International Conference on Intelligent Robots and Systems*. IEEE, 2014, pp. 1846–1853.
- [3] J. Salvi, X. Armangué, and J. Batlle, "A comparative review of camera calibrating methods with accuracy evaluation," *Pattern recognition*, vol. 35, no. 7, pp. 1617–1635, 2002.
- [4] E. A. Martínez-García, J. Domínguez, and R. Lavrenov, "Dynamic modelling and control of an underactuated klann-based hexapod," in *2019 12th International Conference on Developments in eSystems Engineering (DeSE)*. IEEE, 2019, pp. 64–69.
- [5] M. Fiala and C. Shu, "Fully automatic camera calibration using self-identifying calibration targets," *Techn. Rep.*, vol. 48306, p. 26, 2005.
- [6] J. Suriansky and M. Cmarada, "Analysis of methods for camera calibration in 3d scanning systems," *Annals & Proceedings of DAAAM International*.–2012, 2012.
- [7] Z. Zhang, "Camera calibration," *Computer vision: a reference guide*, pp. 76–77, 2014.
- [8] J. Kannala, J. Heikkilä, and S. S. Brandt, "Geometric camera calibration," *Wiley Encyclopedia of Computer Science and Engineering*, vol. 13, no. 6, pp. 1–20, 2008.

- [9] F. Remondino and C. Fraser, "Digital camera calibration methods: considerations and comparisons," *International Archives of Photogrammetry, Remote Sensing and Spatial Information Sciences*, vol. 36, no. 5, pp. 266–272, 2006.
- [10] B. Atcheson, F. Heide, and W. Heidrich, "Caltag: High precision fiducial markers for camera calibration," in *VMV*, vol. 10, 2010, pp. 41–48.
- [11] A. Sagitov, K. Shabalina, L. Sabirova, H. Li, and E. Magid, "Arttag, apriltag and caltag fiducial marker systems: Comparison in a presence of partial marker occlusion and rotation," in *ICINCO (2)*, 2017, pp. 182–191.
- [12] R. Polvara, M. Patacchiola, S. Sharma, J. Wan, A. Manning, R. Sutton, and A. Cangelosi, "Toward end-to-end control for uav autonomous landing via deep reinforcement learning," in *2018 International Conference on Unmanned Aircraft Systems (ICUAS)*. IEEE, 2018, pp. 115–123.
- [13] S. Basiratzadeh, E. D. Lemaire, M. Dorrikhteh, and N. Baddour, "Fiducial marker approach for biomechanical smartphone-based measurements," in *2019 3rd International Conference on Bio-engineering for Smart Technologies (BioSMART)*. IEEE, 2019, pp. 1–4.
- [14] D. Khan, S. Ullah, D.-M. Yan, I. Rabbi, P. Richard, T. Hoang, M. Billinghurst, and X. Zhang, "Robust tracking through the design of high quality fiducial markers: an optimization tool for artoolkit," *IEEE access*, vol. 6, pp. 22 421–22 433, 2018.
- [15] D. Khan, S. Ullah, and I. Rabbi, "Factors affecting the design and tracking of artoolkit markers," *Computer Standards & Interfaces*, vol. 41, pp. 56–66, 2015.
- [16] M. Fiala, "Designing highly reliable fiducial markers," *IEEE Transactions on Pattern analysis and machine intelligence*, vol. 32, no. 7, pp. 1317–1324, 2009.
- [17] F. J. Romero-Ramire, R. Munoz-Salinas, and R. Medina-Carnicer, "Fractal markers: a new approach for long-range marker pose estimation under occlusion," *IEEE Access*, vol. 7, pp. 169 908–169 919, 2019.
- [18] M. Kalaitzakis, S. Carroll, A. Ambrosi, C. Whitehead, and N. Vitzilaios, "Experimental comparison of fiducial markers for pose estimation," in *2020 International Conference on Unmanned Aircraft Systems (ICUAS)*. IEEE, 2020, pp. 781–789.
- [19] A. Zakiev, T. Tsoty, K. Shabalina, E. Magid, and S. K. Saha, "Virtual experiments on aruco and apriltag systems comparison for fiducial marker rotation resistance under noisy sensory data," in *2020 International Joint Conference on Neural Networks (IJCNN)*. IEEE, 2020, pp. 1–6.
- [20] O. Kroeger, J. Huegle, and C. A. Niebuhr, "An automatic calibration approach for a multi-camera-robot system," in *2019 24th IEEE International Conference on Emerging Technologies and Factory Automation (ETFA)*. IEEE, 2019, pp. 1515–1518.
- [21] Y.-C. Tai, Y.-Y. Hsieh, and J.-H. Chuang, "A fully automatic approach for fisheye camera calibration," in *2018 IEEE Visual Communications and Image Processing (VCIP)*. IEEE, 2018, pp. 1–4.
- [22] H. Zhang, K. W. Kwan-yeo, and G. Zhang, "Camera calibration from images of spheres," *IEEE Transactions on Pattern Analysis and Machine Intelligence*, vol. 29, no. 3, pp. 499–502, 2007.
- [23] J. Liu, Z. Yang, H. Huo, and T. Fang, "Camera calibration method with checkerboard pattern under complicated illumination," *Journal of Electronic Imaging*, vol. 27, no. 4, p. 043038, 2018.
- [24] I. Moskvin and R. Lavrenov, "Modeling tracks and controller for servosila engineer robot," in *Proceedings of 14th International Conference on Electromechanics and Robotics "Zavalishin's Readings"*. Springer, 2020, pp. 411–422.
- [25] P. Corke, *Robotics, Vision and Control: Fundamental Algorithms In MATLAB® Second, Completely Revised*. Springer, 2017, vol. 118.
- [26] T. Tsoty, A. Zakiev, K. Shabalina, R. Safin, E. Magid, and S. K. Saha, "Validation of fiducial marker systems performance with rescue robot servosila engineer onboard camera in laboratory environment," in *2019 12th International Conference on Developments in eSystems Engineering (DeSE)*. IEEE, 2019, pp. 495–499.